# Synthesis and Characterization of Low-Melting, Highly Volatile Magnesium MOCVD Precursors and Their Implementation in MgO Thin Film Growth

Lian Wang, Yu Yang, Jun Ni, Charlotte L. Stern, and Tobin J. Marks*

*Department of Chemistry and the Materials Research Center, Northwestern University, Evanston, Illinois 60208-3113*

*Received June 10, 2005. Revised Manuscript Received July 17, 2005*

A series of low-melting, highly volatile, and thermally/air stable diamine-coordinated magnesium metal−organic chemical vapor deposition (MOCVD) precursors, $Mg(hfa)_2$(diamine) and $Mg(hfa)_3H$(diamine) (hfa = 1,1,1,5,5,5-hexafluoro-2,4-pentanedionate), has been synthesized in a single-step aqueous reaction under ambient conditions, and the molecular structures have been determined by single-crystal X-ray diffraction. These fluorocarbon-bearing magnesium complexes exhibit significantly lower melting points and higher volatilities than most previously reported magnesium precursors for MgO thin film growth. One complex of the series, bis(1,1,1,5,5,5-hexafluoro-2,4-pentanedionato)(*N*,*N*,*N*′,*N*′-tetramethylethylenediamine)magnesium(II), with a low melting point (61 °C) and excellent volatility, was successfully implemented in MgO thin film growth by MOCVD. Phase-pure MgO thin films were deposited on Corning 1737F glass, single-crystal Si, and single-crystal $SrTiO_3$(100) and -(110), over the temperature range 550−675 °C. It is demonstrated that highly (100)-oriented MgO films can be obtained on amorphous glass (X-ray diffraction fwhm = 3.1°). Compared to films on glass, epitaxial MgO thin films on both $SrTiO_3$ substrates exhibit excellent out-of-plane alignment (fwhm = 0.7 and 0.9°) and good in-plane alignment. The microstructures, surface morphologies, and optical properties of the MgO thin films were also investigated as a function of growth temperature.

## Introduction

Magnesia, MgO, is used extensively in the insulating and buffer layers of multilayer electronic/photonic devices due to its very large band gap (7.2 eV), excellent thermal stability (melting point = 2900 °C), electrical insulating properties (dielectric constant = 9.8), and the tendency to form films with highly MgO(100)-oriented textured microstructures, benefiting from the simple cubic rock-salt crystal structure.[1−6] Highly biaxial-textured MgO thin films have been successfully deposited by ion beam-assisted deposition (IBAD) and employed as template/buffer layers for YBCO superconducting coatings, to facilitate templating processes, block electrical crosstalk, and minimize interfacial diffusion and lattice mismatches.[7,8] Textured MgO thin films are also commonly used to improve the thin film crystallinity in magnetic storage media at reduced substrate cost.[9,10] Single-crystal MgO wafers are excellent substrates for epitaxial thin film growth owing to the favorable surface conditions, propagating the desired microstructural texture from the substrate to the films.[11,12] In addition, MgO thin films, with superb refractory properties and low sputtering rates, play an important role as protective layers to ameliorate discharge characteristics and panel lifetime deficiencies in ac-plasma display panels.[13−15]

To date, MgO thin films have been deposited by several techniques, including sol−gel,[3,13,16,17] sputtering,[14,18,19] pulsed laser deposition (PLD),[2] ion beam-assisted deposition (IBAD),[7,8,15] and chemical vapor deposition (CVD).[20−24] Among these techniques, metal−organic chemical vapor

(1) Huang, R.; Kitai, A. H. *Appl. Phys. Lett.* **1992**, *61*, 1450−1452.
(2) Tarsa, E. J.; English, J. H.; Speck, J. S. *Appl. Phys. Lett.* **1993**, *62*, 2332−2334.
(3) Yoon, J. G.; Kim, K. *Appl. Phys. Lett.* **1995**, *66*, 2661−2663.
(4) Zeng, J. M.; Wang, H.; Shang, S. X.; Wang, Z.; Wang, M. *J. Cryst. Growth* **1996**, *169*, 474−479.
(5) Nam, K. H.; Han, J. G. *Surf. Coat. Technol.* **2003**, *171*, 51−58.
(6) Chen, X. Y.; Wong, K. H.; Mak, C. L.; Yin, X. B.; Wang, M.; Liu, J. M.; Liu, Z. G. *J. Appl. Phys.* **2002**, *91*, 5728−5734.
(7) Wang, C. P.; Do, K. B.; Beasley, M. R.; Geballe, T. H.; Hammond, R. H. *Appl. Phys. Lett.* **1997**, *17*, 2955−2957.
(8) Brewer, R. T.; Atwater, H. A. *Appl. Phys. Lett.* **2002**, *80*, 3388−3390.
(9) Lee, L. L.; Cheong, B. K.; Laughlin, D. E.; Lambeth, D. N. *Appl. Phys. Lett.* **1995**, *67*, 3638−3640.
(10) Kang, K.; Zhang, Z. G.; Papusoi, C.; Suzuki, T. *Appl. Phys. Lett.* **2004**, *84*, 404−406.
(11) Jin, S.; Yang, Y.; Medvedeva, J. E.; Ireland, J. R.; Metz, A. W.; Ni, J.; Kannewurf, C. R.; Freeman, A. J.; Marks, T. J. *J. Am. Chem. Soc.* **2004**, *126*, 13787−13793.
(12) Metz, A. W.; Ireland, J. R.; Zheng, J.-G.; Lobo, R. P. S. M.; Yang, Y.; Ni, J.; Stern, C. L.; Dravid, V. P.; Bontemps, N.; Kannewurf, C. R.; Poeppelmeier, K. R.; Marks, T. J. *J. Am. Chem. Soc.* **2004**, *126*, 8477−8492.
(13) Jung, H. S.; Lee, J. K.; Hong, K. S.; Youn, H. J. *J. Appl. Phys.* **2002**, *92*, 2855−2860.
(14) Lee, J. H.; Eun, J. H.; Park, S. Y.; Kim, S. G.; Kim, H. J. *Thin Solid Films* **2003**, *435*, 95−101.
(15) Yu, Z. N.; Seo, J. W.; Zheng, D. X.; Sun, J. *Surf. Coat. Technol.* **2003**, *163*, 398−404.
(16) Ho, I. C.; Xu, Y. H.; Mackenzie, J. D. *J. Sol.-Gel Sci. Technol.* **1997**, *9*, 295−301.
(17) Chakrabarti, S.; Ganguli, D.; Chaudhuri, S. *Mater. Lett.* **2003**, *57*, 4483−4492.
(18) Caceres, D.; Vergara, I.; Gonzalez, R. *J. Appl. Phys.* **2003**, *93*, 4300−4305.
(19) Cheng, Y. H.; Kupfer, H.; Richter, F.; Giegengack, H.; Hoyer, W. *J. Appl. Phys.* **2003**, *93*, 1422−1427.

10.1021/cm0512528 CCC: $30.25 © 2005 American Chemical Society
Published on Web 10/14/2005

deposition (MOCVD) provides many advantages, including relatively simple apparatus, adaptability to large-scale production, excellent conformal coverage, suitability for a wide range of deposited materials, and accessibility of metastable phases.[20,24] MgO films grown on amorphous glass substrates are typically polycrystalline.[4,24−28] For these reasons, highly crystalline and epitaxial MOCVD-derived MgO films would be of great interest; however, to date this goal has remained elusive. A crucial element for successful thin film growth by MOCVD is the availability of effective metal−organic precursors which can provide a steady vapor pressure and cleanly deliver the metal-containing species to decompose and subsequently achieve phase-pure film growth on the substrates. Thus, there are several criteria, including high volatility, air stability, substantial thermal stability, and low melting point, essential for effective MOCVD precursors. To date, magnesium MOCVD precursors have not been optimally effective due either to high melting points/low volatility or poor thermal stability.[20,29−34] High melting points lead to sintering and falling volatility, requiring large temperature ramps for precursors to maintain acceptable volatility over film growth runs in the former case and instability of precursor delivery rate in the latter. $\beta$-Diketonates have been widely used to improve the volatility and thermal stability of alkaline-earth ions with great success.[35−39] $Mg^{2+}$, an alkaline-earth ion with a small charge-to-radius ratio, generally prefers six coordination to achieve saturation and suppress oligomerization.[29,31,33] Simple $\beta$-diketonate ligands are virtually incapable of saturating the $Mg^{2+}$ coordination sphere, and hence, volatility-depressing oligomerization is frequently observed.[39] To compensate for such coordinative deficiencies, a typical tactic is to introduce neutral ancillary ligands, which are able to sterically/electronically effect coordinative saturation of the center metal.[20,30,35,37,39,40] Polydentate Lewis base ligands and their derivatives are commonly used as neutral ancillary ligands.[39,43] The new fluorine-free $\beta$-diketone diamine complex $Mg(dpm)_2$(TMEDA) (**A**; dpm = 2,2,6,6-tetramethyl-3,5-heptanedionate, TMEDA = *N*,*N*,*N*′,*N*′-tetramethylethylenediamine), was previously reported by this laboratory and was implemented in MgO thin film growth.[20]

**A**

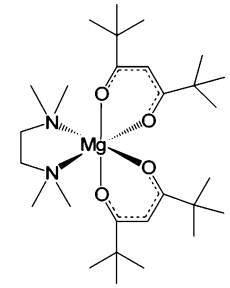


This complex offers moderate volatility and an undesirably high melting point of 212 °C. Thus, there still remains a need for a significantly more effective magnesium MOCVD precursor. It is known that fluorinated $\beta$-diketonate ligands (1,1,1,5,5,5-hexafluoro-2,4-pentanedionate) can be employed to further depress melting points and enhance volatility and thermal stability, and several fluoro $\beta$-diketonato magnesium complexes have been reported.[40] However, their transport/film growth properties and crystal structures are unknown, and the question remains as to whether diamine ancillary ligands could provide well-defined, monomeric precursors with enhanced volatility and stability.

In this contribution, a new class of air-stable magnesium complexes with fluorinated $\beta$-diketonate and various ancillary diamine ligands is synthesized and characterized, and their molecular structures are defined by single-crystal diffraction. The volatilities and thermal stabilities are systematically studied by thermogravimetric analysis (TGA). It is will be seen that these newly developed magnesium MOCVD precursors are lower melting and more volatile than previous precursors and are particularly effective in MgO thin film growth. The resulting phase-pure MgO thin films can be grown on glass, Si, and single-crystal $SrTiO_3$ substrates by MOCVD.

## Experimental Section

**Reagents.** All reagents were used as received. $Mg(NO_3)_2 \cdot 6H_2O$ (99.995% metals basis) was obtained from Aldrich, 1,1,1,5,5,5-hexafluoro-2,4-pentanedione (Hhfa, 98%) was from Oakwood Chemicals, *N*,*N*,*N*′,*N*′-tetramethylethylenediamine (TMEDA, 99.5+%) and *N*,*N*,*N*′,*N*′-tetraethylethylenediamine (TEEDA, 98%) were from

(20) Babcock, J. R.; Benson, D. D.; Wang, A. C.; Edleman, N. L.; Belot, J. A.; Metz, M. V.; Marks, T. J. *Chem. Vapor Deposition* **2000**, *6*, 180−183.
(21) Fan, W.; Markworth, P. R.; Marks, T. J.; Chang, R. P. H. *Mater. Chem. Phys.* **2001**, *70*, 191−196.
(22) Fujii, E.; Tomozawa, A.; Torii, H.; Takayama, R.; Nagaki, M.; Narusawa, T. *Thin Solid Films* **1999**, *352*, 85−90.
(23) Boo, J. H.; Lee, S. B.; Yu, K. S.; Koh, W.; Kim, Y. *Thin Solid Films* **1999**, *341*, 63−67.
(24) Kwak, B. S.; Boyd, E. P.; Zhang, K.; Erbil, A.; Wilkins, B. *Appl. Phys. Lett.* **1989**, *54*, 2542−2544.
(25) Hsu, W. Y.; Raj, R. *Appl. Phys. Lett.* **1992**, *60*, 3105−3107.
(26) Rhee, S. H.; Yang, Y.; Choi, H. S.; Myoung, J. M.; Kim, K. *Thin Solid Films* **2001**, *396*, 23−28.
(27) Sung, M. M.; Kim, C.; Kim, C. G.; Kim, Y. *J. Cryst. Growth* **2000**, *210*, 651−654.
(28) DeSisto, W. J.; Henry, R. L. *Appl. Phys. Lett.* **1990**, *56*, 2522−2523.
(29) Hatanpää, T.; Ihanus, J.; Kansikas, J.; Mutikainen, I.; Ritala, M.; Leskelä, M. *Chem. Mater.* **1999,** *11*, 1846−1852.
(30) Hatanpää, T.; Kansikas, J.; Mutikainen, I.; Leskelä, M. *Inorg. Chem.* **2001,** *40*, 788−794.
(31) Davies, H. O.; Jones, A. C.; Leedham, T. J.; Crosbie, M. J.; Wright, P. J.; Boag, N. M.; Thompson, J. R. *Chem. Vapor Deposition* **2000**, *6*, 71−75.
(32) Matthews, J. S.; Just, O.; Obi-Johnson, B.; Rees, W. S. *Chem. Vapor Deposition* **2000**, *6*, 129−132.
(33) Sung, M. M.; Kim, C. G.; Kim, J.; Kim, Y. *Chem. Mater.* **2002**, *14*, 826−831.
(34) Hill, M. R.; Jones, A. W.; Russell, J. J.; Roberts, N. K.; Lamb, R. N. *J. Mater. Chem.* **2004**, *14*, 3198−3202.
(35) Babcock, J. R.; Wang, A. C.; Metz, A. W.; Edleman, N. L.; Metz, M. V.; Lane, M. A.; Kannewurf, C. R.; Marks, T. J. *Chem. Vapor Deposition* **2001**, *7*, 239−241.
(36) McAleese, J.; Plakatouras, J. C.; Steele, B. C. H. *Thin Solid Films* **1996**, *280*, 152−159.
(37) Darr, J. A.; Drake, S. R.; Hursthouse, M. B.; Malik, K. M. A.; Miller, S. A. S.; Mingos, D. M. P. *J. Chem. Soc., Dalton Trans.* **1997**, 945−950.
(38) Neumayer, D. A.; Belot, J. A.; Feezel, R. L.; Reedy, C.; Stern, C. L.; Marks, T. J. *Inorg. Chem.* **1998**, *37*, 5625−5633.
(39) Otway, D. J.; Rees, W. S. *Coord. Chem. Rev.* **2000**, *210*, 279−328.
(40) Fenton, D. E. *J. Chem. Soc. A* **1971**, *22*, 3481−3485.
(41) Burnett, M. N.; John, C. K. *ORTEP III*; Report ORNL-6895; Oak Ridge National Laboratory: Oak Ridge, TN, 1996.
(42) Hinds, B. J.; Mcneely, R. J.; Studebaker, D. B.; Marks, T. J.; Hogan, T. P.; Schindler, J. L.; Kannewurf, C. R.; Zhang, X. F.; Miller, D. J. *J. Mater. Res.* **1997**, *12*, 1214−1236.
(43) *FILMeasure*, version 2.3.6; Filmetrics, Inc.: 2000. The Cauchy model is a program-defined model for insulators.

Aldrich, and *N*,*N*′-diethyl-*N*,*N*′-dimethylethylenediamine (*N*,*N*′-DE-*N*,*N*′-DMEDA, 96%) and *N*,*N*-diethyl-*N*′,*N*′-dimethylethylenediamine (*N*,*N*-DE-*N*′,*N*′-DMEDA, 96%) were from Pfaltz and Bauer. Deuterated NMR solvents were purchased from Cambridge Isotope Laboratories, Inc.

**Characterization Methods.** Standard $^1$H and $^{19}$F NMR spectra were obtained on a Varian Mercury 400 MHz spectrometer in benzene-$d_6$. The $^1$H chemical shifts were referenced to the residual protonated solvent resonance. The $^{19}$F chemical shifts were referenced to $CFCl_3$ in $CDCl_3$. Elemental analyses were performed by Midwest Microlabs, Inc. (Indianapolis, IN). Melting points were measured in glass capillaries with a MelTemp melting point apparatus. Thermogravimetric analyses (TGA) were performed at a pressure of ∼5 Torr of nitrogen in a TA Instruments SDT 2960 simultaneous DTA-TGA instrument. Weight loss curves were obtained at a temperature ramp rate of 1.5 °C/min.

**General Synthetic Procedure for Mg MOCVD Precursors.** A single-neck, 500 mL round-bottom flask was charged with $Mg(NO_3)_2{\cdot}6H_2O$ (99.995% metals basis; 23.6 mmol), 40 mL of deionized water, and diamine (23.6 mmol; 1.0 equiv). Next, a ∼70 mL reagent solution containing 1,1,1,5,5,5-hexaflouro-2,4-pentanedione (47.2 mmol; 2.0 equiv) and NaOH (47.2 mmol; 2.0 equiv) in 60 mL of ethanol−deionized water (volume ratio = 1:2) was slowly added under constant stirring. The crude product precipitated immediately, and the resultant mixture was stirred for an additional 30 min. The solid was then collected by filtration using a glass frit, washed with deionized water, and dried over $P_4O_{10}$ in a vacuum desiccator for 24 h. The crude product was next purified by reduced-pressure sublimation (40−60 °C/1.3 mTorr) to provide white or light-yellow powders as the target products.

**Bis(1,1,1,5,5,5-hexafluoro-2,4-pentanedionato)(*N*,*N*,*N*′,*N*′-tetramethylethylenediamine)magnesium(II), Mg(hfa)$_2$(TMEDA) (1).** Yield: 66%. Mp: 61−63 °C. $^1$H NMR ($\delta$, $C_6D_6$): 1.74 [s, 4H, $NCH_2CH_2N$], 1.85 [s, 12H, $N(CH_3)_2$], 6.31 [s, 2H, (CO)CH(CO)]. $^{19}$F NMR ($\delta$, $C_6D_6$): 55.53 [s, 6F, $CF_3$]. Anal. Calcd for $C_{16}H_{18}F_{12}MgN_2O_4$: C, 34.65; H, 3.27; N, 5.05; F, 41.11. Found: C, 34.50; H, 3.20; N, 4.90; F, 41.03.

**Bis(1,1,1,5,5,5-hexafluoro-2,4-pentanedionato)(*N*,*N*′-diethyl-*N*,*N*′-dimethylethylenediamine)magnesium(II), Mg(hfa)$_2$(*N*,*N*′-DE-*N*,*N*′-DMEDA) (2).** Yield: 42%. Mp: 47−49 °C. $^1$H NMR ($\delta$, $C_6D_6$): 0.75 [t, 6H, $CH_3$], 1.75 [q, 4H, $NCH_2CH_2N$], 1.91 [s, 6H, $NCH_3$], 2.11 [q, 2H, $NCH_2CH_3$], 2.74 [q, 2H, $NCH_2CH_3$], 6.30 [s, 2H, (CO)CH(CO)]. $^{19}$F NMR ($\delta$, $C_6D_6$): 55.46 [s, 6F, $CF_3$]. Anal. Calcd for $C_{18}H_{22}F_{12}MgN_2O_4$: C, 37.10; H, 3.81; N, 4.81; F, 39.13. Found: C, 37.46; H, 3.95; N, 4.66; F, 38.67.

**Bis(1,1,1,5,5,5-hexafluoro-2,4-pentanedionato)(*N*,*N*-diethyl-*N*′,*N*′-dimethylethylenediamine)magnesium(II), Mg(hfa)$_2$(*N*,*N*-DE-*N*′,*N*′-DMEDA) (3).** Yield: 39%. Mp: 48−50 °C. $^1$H NMR ($\delta$, $C_6D_6$): 0.70 [t, 6H, $CH_3$], 1.87 [s, 6H, $N(CH_3)_2$], 1.93 [t, 2H, $NCH_2CH_2N$], 2.17 [q, 4H, $N(CH_2CH_3)_2$], 2.75 [t, 2H, $NCH_2CH_2N$], 6.35 [s, 2H, (CO)CH(CO)]. $^{19}$F NMR ($\delta$, $C_6D_6$): 55.46 [s, 6F, $CF_3$]. Anal. Calcd for $C_{18}H_{22}F_{12}MgN_2O_4$: C, 37.10; H, 3.81; N, 4.81; F, 39.13. Found: C, 37.10; H, 3.80; N, 4.71; F, 39.08.

**Bis(1,1,1,5,5,5-hexafluoro-2,4-pentanedionato)H(*N*,*N*,*N*′,*N*′-tetraethylethylenediamine)magnesium(II), Mg(hfa)$_3$(HTEEDA) (4).** Yield: 68%. Mp: 80−82 °C. $^1$H NMR ($\delta$, $C_6D_6$): 0.64 [t, 12H, $CH_3$], 2.31 [m, 12H, $(CH_2)_2NCH_2CH_2N(CH_2)_2$], 6.42 [s, 3H, (CO)CH(CO)]. $^{19}$F NMR ($\delta$, $C_6D_6$): 56.31 [s, 9F, $CF_3$]. Anal. Calcd for $C_{25}H_{27}F_{18}MgN_2O_6$: C, 36.67; H, 3.45; N, 3.42; F, 41.77. Found: C, 36.69; H, 3.44; N, 3.41; F, 41.58.

**Single-Crystal X-ray Diffraction Studies.** Single-crystal X-ray data and refinement details for magnesium complexes **1**−**4** were collected on a SMART-1000 CCD area detector with graphite-monochromated Mo Kα radiation at a temperature of 153 K. The colorless crystals were mounted on a glass fiber with viscous oil (Infineum V8512). Using a Bruker SMART detector and processing by SAINT software from Bruker, data were collected in 0.3° oscillations with 15−20 s exposures over a predetermined $\theta$ range. The crystal-to-detector distance was 50.00 mm with the detector at the 28° swing position. Analytical absorption correction was applied, and the data were corrected for Lorentz and polarization effects. The structures were solved by direct methods and expanded using Fourier techniques. All of non-hydrogen atoms were refined anisotropically except for disordered atoms. Hydrogen atoms were included in idealized positions but not refined. The single-crystal structure plots were drawn using the ORTEP program.[41] All related crystallographic information is summarized in Tables 1−4 and the Supporting Information. The asymmetric unit cell of complex **4** contains two crystallographically dependent parts which will be specifically discussed later.

**Table 1. Crystallographic Data for Complexes 1 and 2**

| param | **1** | **2** |
|---|---|---|
| empirical formula | $C_{16}H_{18}F_{12}MgN_2O_4$ | $C_{18}H_{22}F_{12}MgN_2O_4$ |
| fw | 642.72 | 582.69 |
| temp, K | 153(2) | 153(2) |
| $\lambda$(Mo Kα) radiatn, Å | 0.710 73 | 0.710 73 |
| cryst system | monoclinic | monoclinic |
| space group | *C*2/*c* | $P2_1/c$ |
| unit cell dimens, Å | | |
| *a* | 9.1241(14) | 10.985(2) |
| *b* | 14.6756(14) | 13.6047(18) |
| *c* | 17.772(2) | 16.897(3) |
| unit cell angles, deg | | |
| α | 90.0 | 90.0 |
| $\beta$ | 102.225(3) | 90.479(14) |
| $\gamma$ | 90.0 | 90.0 |
| *V*, Å$^3$ | 2325.7(5) | 2525.1(7) |
| *Z* | 4 | 4 |
| $D_{calcd}$, g/cm$^3$ | 1.584 | 1.533 |
| *F*(000) | 1120 | 1184 |
| reflcns collcd/unique | 10 474/2823 [$R_{int}$ = 0.1534] | 23 242/6159 [$R_{int}$ = 0.0352] |
| largest diff peak and hole (e$^-$/Å$^3$) | 0.358 and −0.297 | 0.919 and −0.558 |
| R[a] | 0.0504 | 0.0800 |
| $R_w$[a] | 0.1347 | 0.2286 |

[a] $R1 = \Sigma||F_o| - |F_c||/\Sigma|F_o|$ and $wR^2 = \{\Sigma[w(F_o^2 - F_c^2)^2]/\Sigma[w(F_o^2)^2]\}^{1/2}$, where $w = 1/[\omega^2(F_o^2) + (0.1551P)^2 + 0.0000P]$ and $P = (F_o^2 + 2F_c^2)/3$.

**MgO Thin Film Growth.** MgO thin film growth was carried out in the previously reported low-pressure, horizontal cold-wall MOCVD reactor.[42] The precursor reservoir containing complex **1**, Mg(hfa)$_2$(TMEDA), was maintained at 41 °C with an ultrahigh purity Ar carrier gas flow rate of 8−30 sccm. The ultrahigh-purity $O_2$ oxidizing gas, bubbled at a flow rate of 400 sccm through deionized water, was mixed with the precursor stream immediately upstream of the susceptor in the reactor. The total system growth pressure was maintained at 4.2 ± 0.1 Torr. Corning 1737F glass, single-side polished single-crystal Si(100), and double-side polished single-crystal $SrTiO_3$ were purchased from Precision Glass and Optics, Montco Silicon Tech., and MTI Crystal Corp., respectively. Before thin film growth experiments, Si substrates were cleaned by immersion in "piranha" solution (concentrated $H_2SO_4$:30% $H_2O_2$ = 7:3 v/v) at 80 °C for 1 h. After cooling of the samples to room temperature, they were rinsed repeatedly with deionized water and immediately dried in an oven at 120 °C. Other substrates were cleaned with acetone and 2-propanol prior to the film deposition. Substrates were placed on a SiC-coated MOCVD susceptor and finally transferred to the quartz susceptor holder of the MOCVD reactor having a laminar flow chamber. The MOCVD susceptor temperature ranged from 550 to 675 °C.

**Table 2. Crystallographic Data for Complexes 3 and 4**

| param | 3 | 4 |
|---|---|---|
| empirical formula | $C_{18}H_{22}F_{12}MgN_2O_4$ | $C_{25}H_{27}F_{18}MgN_2O_6$ |
| fw | 582.69 | 817.80 |
| temp, K | 153(2) | 153(2) |
| $\lambda$(Mo K$\alpha$) radiatn, Å | 0.710 73 | 0.710 73 |
| cryst system | monoclinic | monoclinic |
| space group | $P2_1/c$ | $P2_1/n$ |
| unit cell dimens, Å | | |
| $a$ | 14.241(4) | 12.170(5) |
| $b$ | 10.358(3) | 15.244(6) |
| $c$ | 18.104(5) | 19.126(7) |
| unit cell angles, deg | | |
| $\alpha$ | 90.0 | 90.0 |
| $\beta$ | 110.074(4) | 100.156(6) |
| $\gamma$ | 90.0 | 90.0 |
| $V$, Å$^3$ | 2508.4(11) | 3493(2) |
| $Z$ | 4 | 4 |
| $D_{calcd}$, g/cm$^3$ | 1.543 | 1.555 |
| $F$(000) | 1184 | 1652 |
| reflcns collcd/unique | 22 766/6098 [$R_{int}$ = 0.0453] | 30 878/8390 [$R_{int}$ = 0.0298] |
| largest diff peak and hole (e$^-$/Å$^3$) | 0.635 and −0.404 | 0.712 and −0.566 |
| R[a] | 0.0646 | 0.0727 |
| $R_w$[a] | 0.1823 | 0.1949 |

[a] $R1 = \Sigma||F_o| - |F_c||/\Sigma|F_o|$ and $wR^2 = \{\Sigma[w(F_o^2 - F_c^2)^2]/\Sigma[w(F_o^2)^2]\}^{1/2}$, where $w = 1/[\omega^2(F_o^2) + (0.1551P)^2 + 0.0000P]$ and $P = (F_o^2 + 2F_c^2)/3$.

**Table 3. Selected Bond Distances (Å) and Angles (deg) for Complexes 1−3[a]**

| param | 1 | 2 | 3 |
|---|---|---|---|
| Bond Distances | | | |
| Mg(1)−O(1) | 2.0428(13) | 2.0476(19) | 2.044(2) |
| Mg(1)−O(2) | 2.0428(13) | 2.066(2) | 2.078(3) |
| Mg(1)−O(3) | 2.0610(15) | 2.069(2) | 2.051(2) |
| Mg(1)−O(4) | 2.0610(15) | 2.0439(19) | 2.037(2) |
| Mg(1)−N(1) | 2.2270(17) | 2.233(2) | 2.281(3) |
| Mg(1)−N(2) | 2.2270(17) | 2.230(3) | 2.219(3) |
| Bond Angles | | | |
| O(1)−Mg−O(2) | 85.60(5) | 85.28(8) | 84.91(9) |
| O(1)−Mg−O(3) | 91.97(9) | 90.63(8) | 90.12(9) |
| O(1)−Mg−O(4) | 90.22(6) | 174.29(8) | 174.27(10) |
| O(1)−Mg−N(1) | 92.97(6) | 93.90(9) | 91.67(10) |
| O(1)−Mg−N(2) | 173.58(6) | 90.13(9) | 94.76(10) |
| O(2)−Mg−O(3) | 90.22(6) | 87.00(8) | 88.51(10) |
| O(2)−Mg−O(4) | 173.99(9) | 90.81(8) | 91.49(9) |
| O(2)−Mg−N(1) | 94.25(6) | 95.35(9) | 171.39(10) |
| O(2)−Mg−N(2) | 90.28(6) | 174.95(9) | 90.74(11) |
| O(3)−Mg−O(4) | 85.60(5) | 85.00(7) | 85.32(9) |
| O(3)−Mg−N(1) | 173.58(6) | 175.05(9) | 99.42(11) |
| O(3)−Mg−N(2) | 92.97(6) | 95.18(9) | 174.98(11) |
| O(4)−Mg−N(1) | 90.28(6) | 90.60(8) | 92.50(10) |
| O(4)−Mg−N(2) | 94.25(6) | 93.91(9) | 89.74(10) |
| N(1)−Mg−N(2) | 82.41(9) | 82.83(10) | 81.66(11) |

[a] In complex 1, O(3) is O1_2, O(4) is O2_2, and N(2) is N1_2.

**Thin Film Physical Characterization.** Film thickness was measured with a Tencor P-10 step profilometer after etching a step in the film with dilute nitric acid. X-ray diffraction (XRD) $\theta-2\theta$ scans of MgO thin films on glass were obtained with a Rigaku DMAX-A diffractometer using Ni-filtered Cu K$\alpha$ radiation. High-resolution XRD $\theta-2\theta$ scans, rocking curves, and $\phi$ scans of MgO films on single-crystal $SrTiO_3$ substrates, and rocking curves of MgO thin films on glass as well, were obtained on a home-built Rigaku four-circle diffractometer with detector-selected Cu K$\alpha$ radiation. X-ray photoelectron spectroscopy (XPS) was performed on an Omicron ESCAPROBE system using Al K$\alpha$ radiation. Film surface morphology was imaged on a Digital Instruments Nanoscope III atomic force microscope (AFM). Optical transmittance spectra were acquired using a Cary 500 UV−vis−near-IR spectrophotometer from 300 to 3300 nm and referenced to the spectrum of uncoated Corning 1737F glass substrate. Optical reflectance spectra and the refractive index of MgO thin films was investigated with a Filmetrics F20 thin-film Measurement System (Filmetrics, Inc.). Refractive index was simulated with a Cauchy model based on the reflectance data.[43]

**Table 4. Selected Bond Distances (Å) and Angles (deg) for Complex 4**

| | | | |
|---|---|---|---|
| Bond Distances | | | |
| Mg(1)−O(1) | 2.057(2) | Mg(1)−O(4) | 2.071(2) |
| Mg(1)−O(2) | 2.045(2) | Mg(1)−O(5) | 2.059(2) |
| Mg(1)−O(3) | 2.060(2) | Mg(1)−O(6) | 2.052(2) |
| Bond Angles | | | |
| O(1)−Mg−O(2) | 87.01(9) | O(2)−Mg−O(6) | 93.91(10) |
| O(1)−Mg−O(3) | 90.61(9) | O(3)−Mg−O(4) | 85.61(8) |
| O(1)−Mg−O(4) | 176.01(9) | O(3)−Mg−O(5) | 89.64(9) |
| O(1)−Mg−O(5) | 95.27(9) | O(3)−Mg−O(6) | 173.30(10) |
| O(1)−Mg−O(6) | 94.92(9) | O(4)−Mg−O(5) | 85.96(9) |
| O(2)−Mg−O(3) | 90.14(10) | O(4)−Mg−O(6) | 88.94(9) |
| O(2)−Mg−O(4) | 91.75(9) | O(5)−Mg−O(6) | 86.09(10) |
| O(2)−Mg−O(5) | 177.71(10) | | |

**Scheme 1. Synthesis of Mg(hfa)$_2$(diamine) Complexes and Their Melting Points**

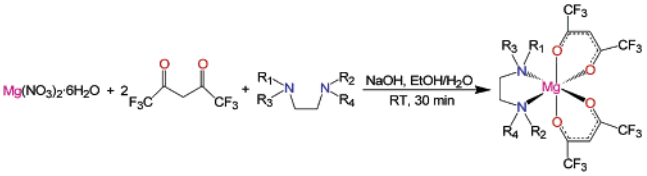


**Scheme 2. Synthesis of the (HTEEDA)$^+$Mg(hfa)$_3^-$ Complex and Its Melting Point**

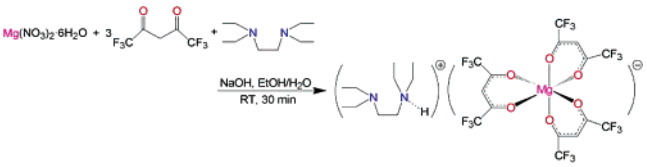


## Results and Discussion

In this section, the syntheses of newly developed Mg(hfa)$_2$(diamine) and Mg(hfa)$_3^-$Hdimaine$^+$ MOCVD precursors are first described, followed by a discussion of their solution phase structures, solid-state structures, and volatility characteristics. Next, the implementation of a particularly effective magnesium precursor in a simple, effective, low-pressure MOCVD growth process for phase-pure MgO thin films is presented. The microstructure, epitaxy, morphology, and optical properties of the MgO thin films are then discussed.

**Magnesium MOCVD Precursor Synthesis and Structural Characterization.** A series of magnesium complexes was prepared in a one-pot synthesis using commercially available reagents (Schemes 1 and 2). The synthesis is carried out in a single-step aqueous reaction with the four selected diamine coligands under ambient conditions. The crude products are insoluble in the $H_2O$/EtOH reaction mixture solution, so are readily collected by filtration and then purified by simple reduced-pressure sublimation at 40−60 °C/1.3 mTorr. The target products are completely solvent-free, despite the fact that the syntheses were carried out in an aqueous medium and that several other solvents are utilized. All target products are air-, light-, and moisture-stable. These complexes are either colorless or light-yellow

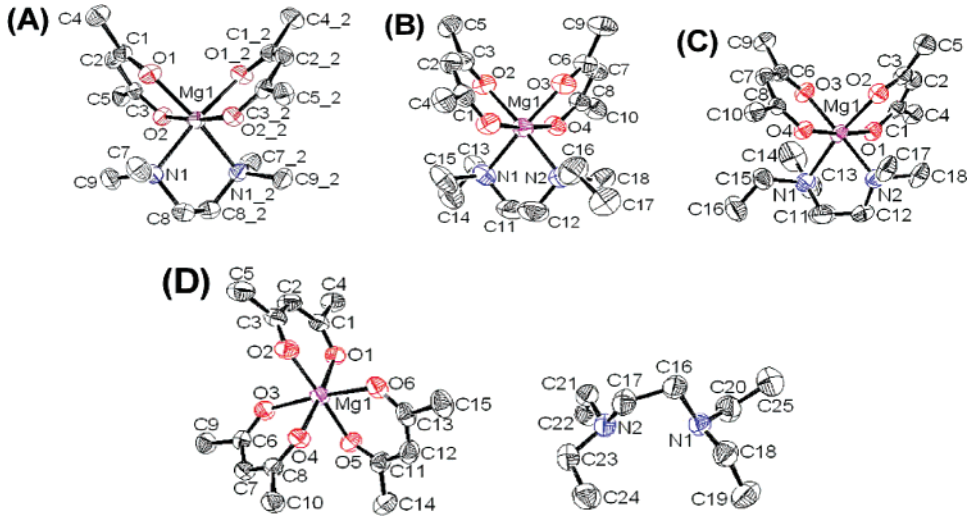


**Figure 1.** ORTEP drawings (50% ellipsoidal probability) of the molecular structures of (A) complex **1**, $Mg(hfa)_2(TMEDA)$, (B) complex **2**, $Mg(hfa)_2$-(*N*,*N*′-DE-*N*,*N*′-DMEDA), (C) complex **3**, $Mg(hfa)_2$(*N*,*N*-DE-*N*′,*N*′-DMEDA), and (4) complex **4**, $Mg(hfa)_3$(HTEEDA). Hydrogen, fluorine, and disordered carbon atoms are omitted for clarity.

powders at room temperature. All new magnesium complexes were characterized by elemental analysis, $^1$H and $^{19}$F NMR spectroscopy, TGA, and single-crystal X-ray diffraction.

The melting points as a function of specific diamine ligand are summarized in Schemes 1 and 2. The melting points of these magnesium complexes vary from 47 to 80 °C and are significantly lower than those of two previously reported fluorine-free magnesium precursors, $Mg(dpm)_2(TMEDA)$ (212 °C) and $Mg(dpm)_2$ (180 °C), implying that the hfa ligand is effective in lowering the melting point vs the dpm ligand. Substituent effects at the periphery of the diamine ligands afford a dispersion in melting points. It can be seen that the symmetry of alkyl group dispositions on the diamines and the structures of the resulting complexes influence the melting points. Note that complex **4** has the highest melting point in the series due to its ionic structure, which will be discussed below.

The $^1$H and $^{19}$F NMR spectra of complexes **1**−**4** imply a consistency with, in each case, a single species being present in solution. For complex **4**, $^1$H NMR shows a single resonance at $\delta$ 6.42 originating from three (CO)CH(CO) protons of the hfa ligand, instead of two protons in the case of complexes **1**−**3**. This peak is shifted downfield relative to the $\delta$ 6.30−6.35 of complexes **1**−**3**. Similarly, in the $^{19}$F NMR spectra, a single resonance at $\delta$ 56.31 originating from the $-CF_3$ groups of complex **4** also shifts downfield relative to $\delta$ 55.46−55.53 for complexes **1**−**3**. The downfield shifts of the hfa ligand $^1$H and $^{19}$F resonances of complex **4** argue (assuming a static structure) that *three* hfa ligands are directly coordinated to the $Mg^{2+}$ center. That is, all hfa ligands in complex **4** are deprotonated and are in the same chemical environment. To maintain the electroneutrality of complex **4**, a diamine nitrogen atom must presumably be protonated and functions as a counterion. While this N−H structural formulation is not directly evidenced by NMR, presumably because of rapid proton exchange/quadrapolar broadening, the single-crystal structure of complex **4** confirms it as shown below.

Single crystals of all complexes suitable for diffraction studies were grown either by slow evaporation of hexane solutions or by reduced-pressure sublimation. Single-crystal X-ray diffraction results confirm that all of the complexes are monomeric, a favorable characteristic for optimum volatility, as shown in Figure 1. Crystallographic data, selected bond lengths, and selected bond angles are summarized in Tables 1−4. In all complexes, the hfa ligands are coordinated to the $Mg^{2+}$ center in a bidentate geometry with planar $\pi$-delocalized $hfa^-$ $(CO)CH(CO)^-$ frameworks. In complexes **1**−**3**, the $Mg^{2+}$ ion is surrounded by two $\beta$-diketonate ligands and one diamine ligand in a distorted-octohedral 6-coordinate geometry. The Mg−N bond lengths in the symmetrical diamine of complex **1** are identical (2.2270(17) Å). Similarly, complex **2** has a quasi-symmetrical diamine, so that the two Mg−NMe(Et) bond lengths are very similar (2.233(2) and 2.230(3) Å). However, the asymmetry of the diamine in complex **3** leads to an inequality of two Mg−N bonds, namely an elongation of $Mg-NEt_2$ to 2.281(3) Å and a corresponding shrinkage of $Mg-NMe_2$ to 2.219(3) Å. This modest variation in the above Mg−N bond lengths can be explained by the bulkiness of the different alkyl substituents. In addition, the average Mg−N bond lengths of complexes **1**−**3** (2.2270(17), 2.2315(25), and 2.250(3) Å, respectively) are shorter than those of $Mg(dpm)_2$-(TMEDA) (averaging 2.2815(20),[20] 2.2765(25) Å[30]) even though the present diamine ligands are sterically comparable to, or greater than, TMEDA. This difference doubtless results from the electron-withdrawing capacity of the fluorocarbon substituents and the resulting enhanced Lewis acidity of the $Mg^{2+}$ center. This effect is also manifested in a slight expansion of the N−Mg−N bond angles. Thus, the N−Mg−N angles in complexes **1**−**3** (82.41, 82.82, and 81.66°, respectively) are slightly larger than in $Mg(dpm)_2(TMEDA)$ (79.51,[20] 79.24°[30]), plausibly because shortening of the Mg−N bonds and the encumbered dpm ligand enhance interligand repulsion. One of the most interesting structural aspects of this series of complexes concerns the observation that complex **4** has a significantly different coordination

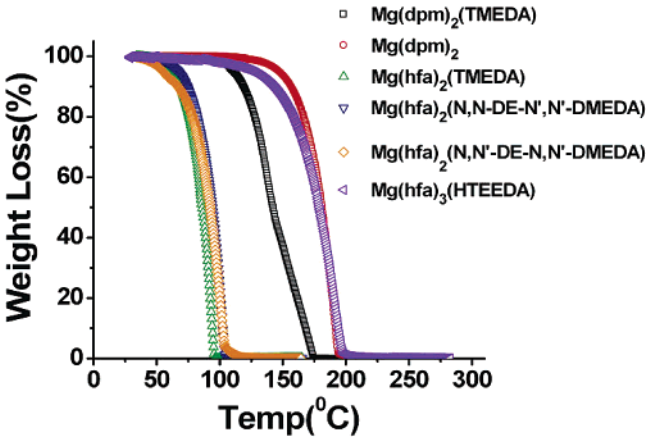


**Figure 2.** Reduced-pressure TGA comparison of the volatilities of Mg(dpm)$_2$(TMEDA), Mg(dpm)$_2$, and the present magnesium complexes. The data were collected at a temperature ramp of 1.5 °C/min under 5 Torr $N_2$ pressure.

**Scheme 3. Detailed Crystallographic Information of the [HTEEDA]$^+$ Part of Complex 4**

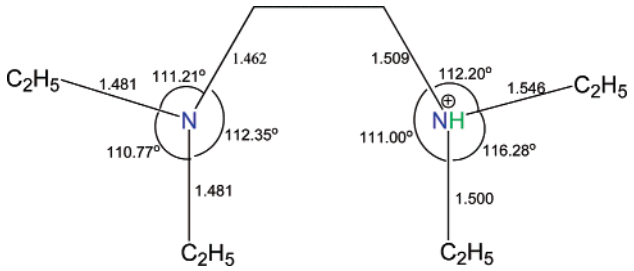


environment in which the diamine ligand does not bind directly to the metal atom but rather serves as a protonated counterion to an anionic Mg(hfa)$_3^-$ species (Figure 1D). Close inspection of the diamine component reveals that one C−N−C angle is much larger (116.28°) than others (averaging 112°), as shown in Scheme 3, indicating that this nitrogen atom is protonated. Unlike previously reported hydrogen-bonding effects in formally analogous alkaline earth diketonate ion-pair complexes,[37,44,45] the shortest N···O and N···F distances in complex **4** are too long to indicate a hydrogen bonding interaction (4.428 Å for N···O and 3.502 Å for N···F). Thus, complex **4** consists of an (Mg(hfa)$_3$)$^-$ anion and a (HTEEDA)$^+$ cation. This stoichiometry between the center metal cation and ligands is in good agreement with NMR spectroscopic data and elemental analysis. The anion component contains a chelating six-coordinate magnesium atom bonded directly to three hfa ligands. Therefore, complex **4** is essentially an ionic compound.

**Precursor Volatility.** To quantify precursor volatility characteristics, TGA experiments on magnesium complexes **1**−**4** were performed at ∼5 Torr, approximating the pressure used in the MOCVD film growth process (Figure 2). Comparative TGA data for Mg(dpm)$_2$(TMEDA) and Mg(dpm)$_2$ are also shown in Figure 2. Note that precursors **1**−**4** all exhibit smooth volatilization curves with no significant residue or discontinuities, indicating clean single volatilization processes with negligible ligand decomposition and ensuring constant precursor transport properties in MOCVD growth processes. It can also be seen that complexes **1**−**3** evaporate completely at far lower temperatures (<110 °C) than Mg(dpm)$_2$(TMEDA) (170 °C) and Mg(dpm)$_2$ (190 °C). These superior volatilities will doubtless provide efficient Mg transport to the reactor hot-zone at low temperatures without decomposition and should thus afford compositionally reproducible thin film growth. Complex **4**, however, exhibits more limited volatilization properties, roughly comparable to Mg(dpm)$_2$, which can be explained in terms of the larger molecular weight and greater lattice electrostatic cohesive energies.

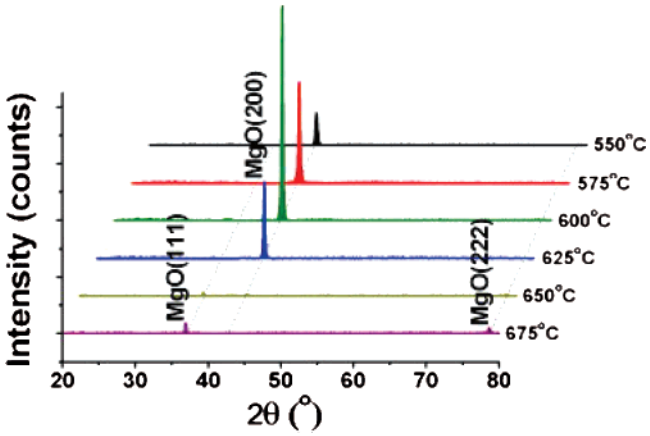


**Figure 3.** X-ray diffraction $\theta-2\theta$ scans of MOCVD-derived MgO films on Corning 1737F glass grown from 550 to 675 °C.

**MgO Thin Film Growth.** MgO thin films were grown on Corning 1737F glass, single-crystal Si, and single-crystal $SrTiO_3$(100) and -(110) substrates by low-pressure MOCVD using metal−organic magnesium precursor **1** due to its excellent volatility and thermal stability. Because of the presence of the fluorinated ligand, the $O_2$ oxidizing gas was saturated with $H_2O$ vapor to minimize the fluoride contamination in the product films. The MgO thin films with thicknesses of 170−200 nm on glass, ∼340 nm on Si, and ∼240 nm on both $SrTiO_3$ substrates were obtained. The optimum growth temperature was determined after some experimentation to be between 550 and 675 °C with a growth rate of 1.5 ± 0.4 nm/min on glass, 600 °C with a growth rate of 1.4 ± 0.1 nm/min on Si, and 600 °C with a growth rate of 1.6 ± 0.1 nm/min on both $SrTiO_3$ substrates. The as-grown films are uniformly colorless, smooth, and extremely transparent.

**MgO Film Texture on Glass Substrates.** X-ray diffraction $\theta-2\theta$ scans of the as-deposited MOCVD-derived MgO thin films on glass substrates were carried out from $2\theta$ = 20−80°. Figure 3 shows the XRD data as a function of the film growth temperature. All films exhibit the cubic rock-salt structure. Diffraction patterns are dominated by a strong (200) reflection for the MgO thin films grown between 550 and 625 °C and gradually evolve into a weak (111) reflection as the growth temperature reaches 675 °C. It is known that the (200) orientation has the lowest surface energy and highest packing density and for other growth techniques is favored at relatively low growth temperatures.[46] Higher growth temperatures induce greater surface energies, so that

(44) Sievers, R. E.; Turnipseed, S. B.; Huang, L.; Lagalante, A. F. *Coord. Chem. Rev.* **1993**, *128*, 285−291.
(45) Hamilton, W. C.; Ibers, J. A. *Hydrogen Bonding in Solids*; W. A. Benjamin: New York, 1968; pp 260−265.

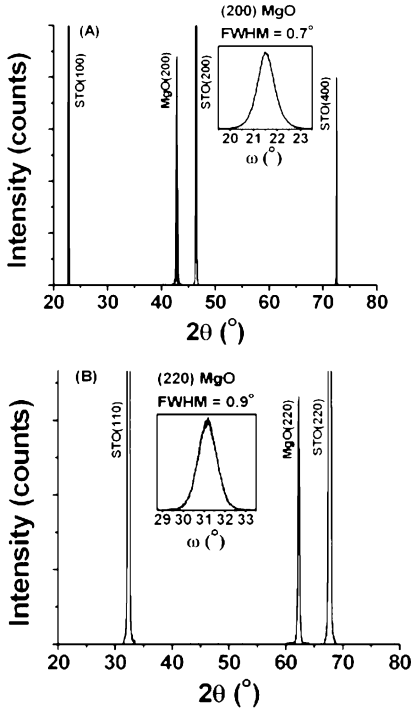


**Figure 4.** High-resolution X-ray diffraction $\theta-2\theta$ scans and the rocking curves (inset) of MOCVD-derived MgO films grown at 600 °C on (A) $SrTiO_3(100)$ and (B) $SrTiO_3(110)$.

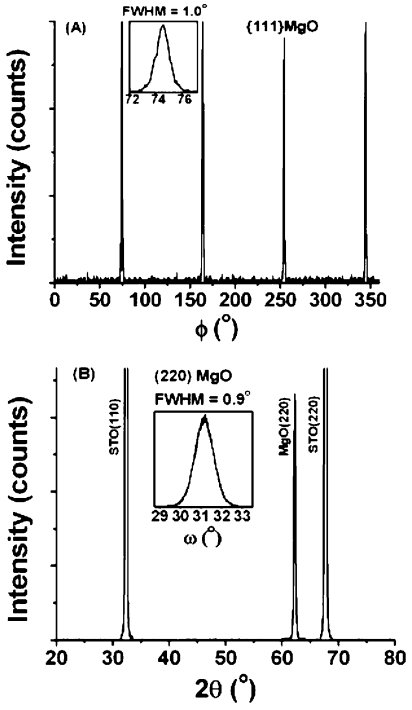


**Figure 5.** High-resolution X-ray diffraction $\phi$-scans and fwhm (inset) of MgO films grown at 600 °C on (A) $SrTiO_3(100)$ and (B) $SrTiO_3(110)$.

the preferred (200) growth orientation gradually evolves into a preferred (111) orientation. For MgO films grown at 600 °C, the full-width at half-maximum (fwhm) of the (200) reflection is a relatively small 3.1°. In addition, a survey of precursor flow rate effects was carried out at the 600 °C growth temperature. Over the flow rate range of 8−30 sccm, the MgO thin films exhibit only the (200) reflection, indicating that the MOCVD-derived MgO film microstructure is relatively insensitive to precursor flow rate.

**MgO Film Epitaxy on Single-Crystal $SrTiO_3$ Substrates.** $SrTiO_3$, with a lattice constant of 3.90 Å (7.5% lattice mismatch with the MgO lattice constant of 4.216 Å), was used as the substrate for the epitaxial MgO thin film growth. Two $SrTiO_3$ substrates, $SrTiO_3(100)$ and $SrTiO_3(110)$, were employed in the present work. The $\theta-2\theta$ scans shown in Figure 4 reveal that single crystalline MgO thin films grown on single-crystal $SrTiO_3$ substrates exhibit a (200) textured microstructure on $SrTiO_3(100)$ and a (220) textured microstructure on $SrTiO_3(110)$. The out-of-plane and in-plane order of the as-grown MgO thin films were further assessed by rocking curves (inset) and $\phi$-scans, respectively, as displayed in Figures 4 and 5, respectively. The rocking curves of the films reveal good out-of-plane alignment of both MgO films (Figure 4), with a fwhm of 0.7° for films grown on $SrTiO_3(100)$ and 0.9° for films grown on $SrTiO_3(110)$. $\phi$-scans were performed to examine the quality of the in-plane epitaxy. The in-plane orientations were investigated using the MgO(111) reflection at $\chi = 54.74°$ for $SrTiO_3(100)$ and the MgO(200) reflection at $\chi = 45°$ for $SrTiO_3(110)$, as shown in Figure 5. In the cubic system, the (100) plane has a 4-fold symmetry repeating every 90°, and the (220) plane has a 2-fold symmetry repeating every 180°. The clean 4-fold rotational symmetry of the MgO(111) reflection and 2-fold rotational symmetry of the MgO(220) reflection exhibit small fwhms of 1.0 and 1.4° for films grown on $SrTiO_3(100)$ and $SrTiO_3(110)$, respectively, implying a high level of in-plane epitaxy. The orientations of the phase-pure MgO thin films on the $SrTiO_3$ substrates thus have the relationships of MgO(100)||$SrTiO_3(100)$ and MgO(110)||$SrTiO_3(110)$.

**MgO Film Composition.** Because of the fluorine-containing ligands present in the magnesium MOCVD precursors, one obvious concern is the possibility of fluoride contamination or fluoride phase formation during the thin film growth process. The most efficient solutions to minimize fluorine content are to introduce the water into the oxidizing gas and to maintain the film growth at relatively high temperatures,[47−49] as was done here. X-ray diffraction indicates that any extraneous fluoride phases are below the detection limits. Fluorine contamination was quantitatively investigated by X-ray photoelectron spectroscopy (XPS). In the present film composition study, the surface layer (∼6 nm) exposed to air was first removed by Ar ion sputtering (2 kV, 10 $\mu$A, sputtering rate at ∼3 Å/min). The fluorine content was then found to be less than 0.6 atom % in the as-grown MgO thin films, and no obvious differences in fluorine content were observed for the different growth substrates. Hence, the fluorine content is minimal in the present MOCVD-derived thin films and should not significantly influence the observed microstructural and optical characteristics.

**Film Morphology.** The surface morphologies of the as-grown MgO thin films were examined by contact-mode AFM, as shown in Figure 6. The AFM images show that

(46) Arendt, P. N.; Foltyn, S. R. *MRS Bull.* **2004**, *29*, 543−550.
(47) Ehrich, H.; Musa, G.; Popescu, A.; Mustata, I.; Salabas, A.; Cretu, M.; Leu, G. F. *Thin Solid Films* **1999**, *344*, 63−66.
(48) McAleese, J.; Steele, B. C. H. *Corros. Sci.* **1998**, *40*, 113−123.
(49) Chadwick, D.; McAleese, J.; Senkiw, K.; Steele, B. C. H. *Appl. Surf. Sci.* **1996**, *99*, 417−420.

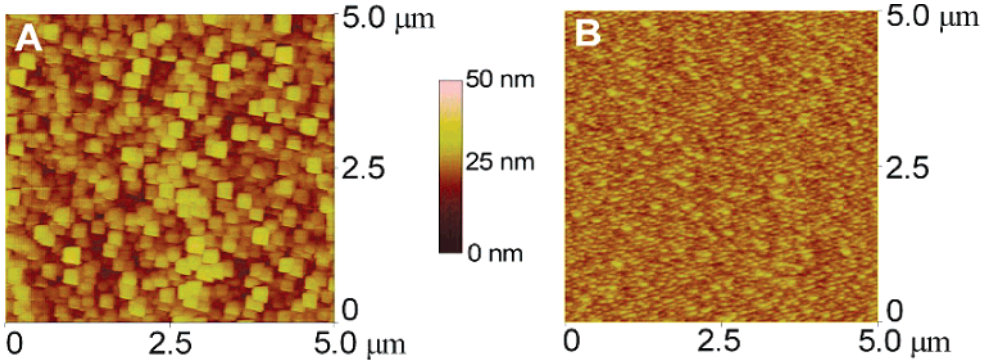


**Figure 6.** AFM images of MOCVD-derived MgO thin films grown at 600 °C with a precursor flow rate of 12 sccm on (A) Corning 1737F glass and (B) $SrTiO_3$(110).

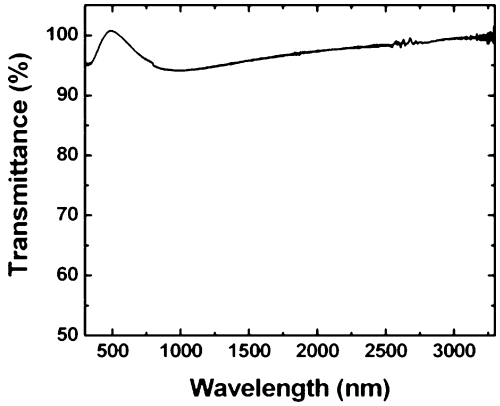


**Figure 7.** UV−vis−NIR transmittance optical spectrum of a ∼170 nm MgO grown at 600 °C on Corning 1737F glass.

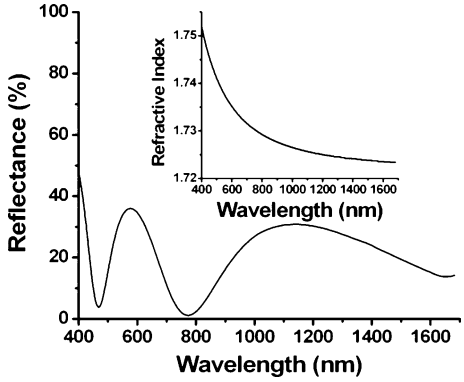


**Figure 8.** Reflectance spectrum and refractive index (inset) of ∼340 nm MgO grown at 600 °C on a Si substrate.

the as-grown MgO thin films are very smooth and densely packed with a grained structure. For a 600 °C growth temperature, Figure 6A shows that MgO films on glass have only square-shaped grains. The MgO thin films on glass exhibit a root-mean-square (rms) roughness of 4−6 nm over $5 \times 5\ \mu m^2$ areas, depending on the growth temperature and magnesium precursor flow rate. The MgO films grown on single-crystal $SrTiO_3$ substrates, with smaller grain sizes, are clearly smoother than those grown on glass and have smaller rms roughnesses (2−2.4 nm) over $5 \times 5\ \mu m^2$ areas as shown in Figure 6B, which is doubtless attributed to the epitaxial growth.

**MgO Thin Film Optical Properties.** The optical properties of present MgO thin films have also been characterized. The as-deposited MgO thin films on glass substrates are colorless and extremely transparent. A typical optical transmission spectrum is shown in Figure 7. MgO thin films with thicknesses of ∼170 nm on glass exhibit very high levels of transparency, averaging >95% over the 300−3300 nm wavelength range. The reflectance spectrum and refractive index (inset) of a ∼340 nm MgO film grown on single-crystal Si are shown as a function of wavelength in Figure 8. The refractive index was computed from the reflectance spectral data. It can be seen that the refractive index decreases slightly from 1.752 at 400 nm to 1.724 at 1700 nm, indicating a substantial dispersion with respect to wavelength.[50,51]

## Conclusions

A series of air-stable, easy-to-handle magnesium MOCVD precursors has been prepared and characterized. These newly developed precursors exhibit substantially lower melting points and greater volatilities than previously reported magnesium MOCVD precursors for MgO thin film growth. The monomeric magnesium complexes are coordinatively saturated with the combination of fluorinated $\beta$-diketonate and neutral bidentate diamine ligands. Substitution of various alkyl moieties on the diamine skeleton offers tailoring of the melting point and volatility characteristics. One of these precursors was successfully implemented in MgO thin film growth. The as-grown MgO films on glass are phase-pure, highly crystalline, and smooth, and should have potential applications as the structural template/insulating layer in multilayer films and devices. Epitaxial MgO films grown on single-crystal $SrTiO_3$ exhibit highly biaxially textured microstructures. The MgO films also exhibit excellent optical transparency.

**Acknowledgment.** We thank the NSF (Grant CHE-0201767) for support of this research. Characterization facilities were provided by the Northwestern University MRSEC program (Grant NSF-DMR-00760097).

**Supporting Information Available:** Detailed crystallographic information for complexes **1**−**4**. This material is available free of charge via the Internet at http://pubs.acs.org.

CM0512528

(50) Teng, C. W.; Muth, J. F.; Ozgur, U.; Bergmann, M. J.; Everitt, H. O.; Sharma, A. K.; Jin, C.; Narayan, J. *Appl. Phys. Lett.* **2000**, *76*, 979−981.
(51) Fang, G. J.; Li, D. J.; Zhao, X. Z. *Phys Status Solidi A* **2003**, *200*, 361−368.